Results in Engineering 22 (2024) 102064

Contents lists available at ScienceDirect

Results in Engineering

journal homepage: www.sciencedirect.com/journal/results-in-engineering

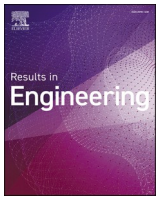

Novel Kuhn-Tucker conditions for vibration analysis in a functionally graded porous beam using the R-program

Geetha Narayanan Kannaiyan [a,b], Vivekanandam Balasubramaniam [a], Bridjesh Pappula [c], Seshibe Makgato [c,*]

[a] Faculty of Computer Science and Multimedia, Lincoln university college, Malaysia
[b] Department of Mathematics, Dayananda Sagar college of engineering, Bengaluru, 560078, India
[c] Department of Chemical Engineering, College of Science, Engineering and Technology, University of South Africa (UNISA), C/o Christiaan de Wet & Pioneer Avenue, Florida Campus, 1710, Johannesburg, South Africa

ARTICLE INFO

Keywords:
Bi-directional functionally graded beam
Kuhn-Tucker conditions
R-Program
Dimensionless natural frequency

ABSTRACT

Functionally graded materials provide a flexible and individualized strategy for material design, allowing for optimization of properties and performance for particular purposes. The investigation considers the effects of simply supported (SS), clamped-clamped (CC) and clamped-free (CF) configurations. The study examines the vibration characteristics of bi-directional functionally graded porous beams (BDFGPB) using the third-order shear deformation theory, considering both even and uneven porosity conditions. The Hamilton method is used to derive equilibrium equations for beams, which are then solved using the Kuhn-Tucker technique and R-program. The BDFGPB's validity was verified by comparing it with open literature, revealing deviations of 3.19%, 1.25%, and 2.15% in non-dimensional natural frequency for SS, CC and CF boundary conditions. Furthermore, as the porosity index increases, the dimensionless natural frequency decreases, reducing beam stiffness and rigidity. This study demonstrates that porosity plays a critical role in the design of modern structures, as its ratio greatly impacts their performance and responsiveness.

1. Introduction

Functionally graded materials (FGMs) are a category of engineered materials that possess a gradual and continual variation in composition, microstructure or properties across the volume. The FGMs are modelled in such a way that the properties may change systematically from one region to another, unlike conventional materials with uniform properties throughout. The continual variation in properties within FGMs allows them to overcome limitations found in traditional homogeneous materials. Designing FGMs allows for a smooth transition from a material with high strength and low thermal expansion to another material with high toughness and high thermal expansion [1]. This gradient in properties helps to minimize stress concentrations and improve the overall performance and reliability of the material [2]. Porous structures introduce voids or empty spaces within the material, affecting its mechanical behaviour and dynamic response. Porosity can vary along the beam's length or cross-section, influencing parameters like mass density, stiffness and damping characteristics. The amount of porosity (porous and non-porous) has an impact on the vibration behaviour of the plate or beam [3–5]. The internal distribution of pores within the structure may exhibit various patterns, such as uniform, non-uniform, trigonometric, exponential and others. FGMs in the biomedical field find application in dental implants [6] and orthopaedic implants [7], in aerospace applications [8], civil engineering [9], Energy absorption devices [10], electronics and electrical engineering [11] and in thermal management applications [12]. Hai Qing and Lu Wei [13] investigated the natural frequency behaviour of functionally graded beams (FGB). They considered different porosity distributions and material property variations across the thickness. Their study used mathematical models and numerical techniques to analyze the natural frequencies occurring in the beams. Another study by Nguyen et al. [14] proposed an approach to predicting the free vibration as well as the mode shapes of FGBs. The approach used two-variable shear deformation theory, porosity distribution functions and a power-law disparity of material properties to obtain analytical solutions.

Engineering structures integrate with other structures, leading to numerous investigations into their mechanical characteristics. Refrafi et al. [15] used HSDT to study buckling behaviour in sandwich plates made of FGMs under hygro-thermal and mechanical loads. Mudhaffar

* Corresponding author.
E-mail address: makgato2001@yahoo.com (S. Makgato).

https://doi.org/10.1016/j.rineng.2024.102064
Received 8 February 2024; Received in revised form 22 March 2024; Accepted 26 March 2024
Available online 29 March 2024

Nomenclature

α	The porosity coefficient ($0 \leq \alpha \leq 0.4$)
m	The presence of metal
c	The presence of ceramic
V_f	Volume fraction of one constituent
p_x	The gradient index describing the behavior of a volume fraction throughout the beam's length
p_z	The gradient index describing the behavior of a volume fraction throughout the beam's thickness
E_a	The Modulus of elasticity
ρ_a	Mass density
U	Axial displacements
W	Transverse displacement
$\varnothing$	The shear slope
$\frac{\partial w_0}{\partial x}$	Bending slope
δU	The potential energy of the strain
δK	The kinetic energy of the strain
M_x	The bending moment
Q_x	The shear force
P_x	The functional characteristics of the material
x	The axial direction
z	The direction of thickness
g	where, θ_i, φ_i, and ψ_i are the three different boundary conditions and
λ	The scalar
ANN	Artificial Neural Network
BDFGPB	Bi-directional Functionally Graded Porous Beam
CC	Clamped - Clamped
CF	Clamped - Free
FEA	Finite Element Analysis
FEM	Finite Element Method
FGB	Functionally Graded Beam
FGPB	Functionally Graded Porous Beam
FGM	Functionally Graded Material
GDQM	General Differential Quadrature Method
HSDT	Higher Order Shear Deformation Theory
HYSDT	Hyperbolic Shear Deformation Theory
KT	Kuhn-Tucker
P/IP-FGSB	Perfect/Imperfect Functionally Graded Sandwich Beams
SS	Simply Supported

et al. [16] analyzed the bending analysis of ceramic-metal plates under stress and viscoelastic foundations. Phuong et al. [17] used the Timoshenko beam theory for the structural analysis of FGBs with porosities. The neutral surface theory was proposed to eliminate coupling effects. In a study by Zhao et al. [18], they offered a modified Fourier series methodology to assess the natural frequency developed in the functionally graded porous beams (FGPB). The method considered the porosity distribution and material property variations across the thickness. Comparisons with numerical results validated the accuracy of the methodology. Van Vinh et al. [19] used the nonlocal elasticity theory into consideration and the consequences on a smaller scale. They deduced the governing equations and further estimated the natural frequencies, as well as the mode, shapes through numerical techniques. A study by Arefi and Meskini [20] proposed a hyperbolic shear deformation theory (HYSDT) to examine the vibration behaviour of FGPBs. They considered material property variations, porosity effects and transverse shear deformation. The free vibration was obtained by applying Navier's method. Another study by Jena et al. [21] studied the vibration phenomenon of FGPB using the modified couple stress theory [11] while considering the impact of porosity and material grading. An analytical approach based on a power series expansion obtained the natural frequencies. Gao et al. [22] examined the influence of uncertain parameters on the vibration behaviour of FGPB. They used a probabilistic approach to model the uncertainties in material properties and porosity. The fuzzy method was employed to analyze the random vibration response and obtain statistical information. Hung et al. [23] assessed the dynamic response of a sandwich beam composed of FGM and graphene platelets. Parametric studies were executed to estimate the impact of the porosity coefficient on the beam's dynamic properties. They used Lagrange's equations and Newmark's acceleration method to derive the governing equations.

Researchers have utilized analytical, numerical and probabilistic techniques to assess the impact of material grading, porosity and the effect of boundary conditions on the dynamic behaviour of such beams and plates. Quang Hung et al. [24] established a mesh-free method for structural analysis and response of intelligent piezoelectric porous beams. They adapted the Halpin–Tsai micro-mechanical model to estimate core properties. Also, they examined boundary conditions, the material parameters' impact on beam deflection, and stresses under mechanical and electrical loads, emphasizing piezoelectricity's impact on static bending regulation. Lim et al. [25] developed a model that accounts for nonlocal strain gradients by integrating a nonlocal integral model and one based on strain gradients. Ebrahimi and Barati [26] utilized an advanced refined beam model of higher order to examine the vibration-damping response of an FG beam that was installed in a Winkler-Pasternak foundation [27]. Sahmani and Aghdam [28] examined the nonlinear vibration as well as bending analysis of nanobeams applying the two-step perturbation technique; microtubes were adapted by She et al. [29], and nanotubes by Gao et al. [30]. Ghazwani et al. [31] studied vibration characteristics of porous functionally graded nanobeams, analyzing four porosity distributions and using Eringen's nonlocal parameter elasticity theory and Hamilton's principle to establish motion equations. They solved eigenvalues with a closed-form solution. Mellal et al. [32] proposed an analytical approach for assessing the free vibration and stability of FGBs supported by variable elastic foundations. Their study focused on three unknown functions, transverse shear stresses, and examined the impact of porosity. Avcar et al. [33] investigated natural frequencies in perfect/imperfect functionally graded sandwich beams supported by elastic foundations, using trigonometric shear deformation theory and Hamilton's principle. Hadji and Avcar [34] introduced a nonlocal HYSDT for the free vibration of porous functionally graded nanobeams, examining the impact of nonlocal parameters on dynamic responses. Al-Shujairi and Mollamahmutoglu [35] and Liu et al. [36] used the general differential quadrature method to study the impact of thermal effects on the Timoshenko beam model.

The study conducted by Guo et al. [37] and Lu et al. [38] utilized the Galerkin approach to investigate the transverse vibration as well as the vibro-buckling properties of a simply supported Euler-Bernoulli beam that is both axially moving and rotating. An investigation was conducted on the fluctuating dynamics of carbon nanotubes by Mohammadian et al. [39], adapting a Timoshenko beam model. Karami et al. [40] utilized the GDQM to investigate the free vibration behaviour of a bi-directionally functionally graded Timoshenko beam featuring a tapered cross-sectional geometry. The Kirchhoff plate was utilized by Mir and Tahani [41] in the study of a resonator composed of a graphene sheet. They employed the Melnikov integral method to derive analytical considerations concerning the occurrence of oscillations. Hadji et al. [42] analyzed the bending and free vibration characteristics of FGPB supported by elastic foundations, finding constant variation in material characteristics throughout thickness. They acknowledged the linear, homogeneous, and isotropic nature of the foundation medium. Dahmane et al. [43] studied the impact of inclined transverse cracking on

Euler-Bernoulli-model defective FGBs, finding factors like porosity values, crack depth, and fracture position significantly influencing natural frequencies. They also studied the dynamic response of wave propagation in bidirectional-graded porous cantilever beams [44]. Hadji et al. [45] studied the impact of pore distribution on free vibration analysis in porous plates using HYSDT. Madan et al. [46] found a negative correlation between grading indices and aspect ratio with limited speed, highlighting the potential of exponential disks for industrial applications. Sayyad et al. [47] used higher-order hyperbolic circular beam theory for static and vibration analysis. Sayyad et al. [48] conducted thermal buckling studies on multi-directional plates, establishing critical material grading indices. Hadji et al. [49] utilized HSDT to evaluate the static response of functionally graded plates, demonstrating its variational consistency and similarity to conventional plate theory across dimensions. Turan et al. [50] used FOSDT to analyze the buckling and natural frequency of FGPB, using Finite Element Method (FEM) and Artificial Neural Network (ANN) methodologies. They used Ritz's method, Lagrange's principle, and the power-law rule to derive equations of motion. Various researchers used FEM to assess free vibrations, discretizing the beam into finite elements and establishing natural frequencies and mode shapes [51–55].

In the light of literature discussed, the studies mentioned focus on the mechanical characteristics of various engineering structures, particularly sandwich plates, ceramic-metal plates and beams made of functionally graded materials (FGMs) and functionally graded porous beams (FGPBs). These studies utilized analytical, numerical, and probabilistic techniques to assess the impact of material grading, porosity and boundary conditions on the dynamic behaviour of such structures. Other studies focused on nonlocal strain gradients, vibration-damping response, mesh-free methods and the impact of thermal effects on beam models. However, to the best of the authors' knowledge, there is no available analysis of vibration in FGB with porous structures, particularly those that utilize Kuhn-Tucker (KT) conditions. The study presents a novel approach using mathematical techniques, including the KT conditions solution and R-program, to analyze the free vibration and equilibrium of a beam made of functionally graded porous material. It explores how factors like boundary conditions, material distribution, porosity, and gradient indices impact the beam's natural frequency. Third-order shear deformation theory is used to evaluate vibrational characteristics, with analysis using the Hamilton formulation accounting for power-law distribution in thickness.

2. Theory and formulation

2.1. Formulation of BDFGPB

The current investigation focuses on a beam that demonstrates functional grading, possessing a length L and a rectangular cross-sectional shape characterized by its width 'b' and height 'h'. Fig. 1 depicts the spatial dimensions of the beam represented by the *x*-, *y*- and *z*-coordinates, which correspond to the horizontal direction, the transverse direction and the longitudinal direction, respectively. Generally, functionally graded materials consist of ceramics and metal, with ceramics being a structural material that can withstand high heat and low heat transfer constant, and metal offering flexibility. As depicted in Fig. 1, the BDFGPB is comprised of ceramic at the top and metal at the bottom. The material composition varies along the thickness of the beam according to a power law formulation. Additionally, the porosity of the beam is described as either even or uneven. The consideration of two porosity distribution patterns, even and uneven, in this study, is for a simplification aimed at comparing the effects of porosity patterns on material properties by exploring fundamental aspects of material behaviour which are analytically tractable. This allows for a clearer understanding of how different distribution patterns influence mechanical behaviours.

The BDFGPB is restricted to the behaviour of materials that exhibit

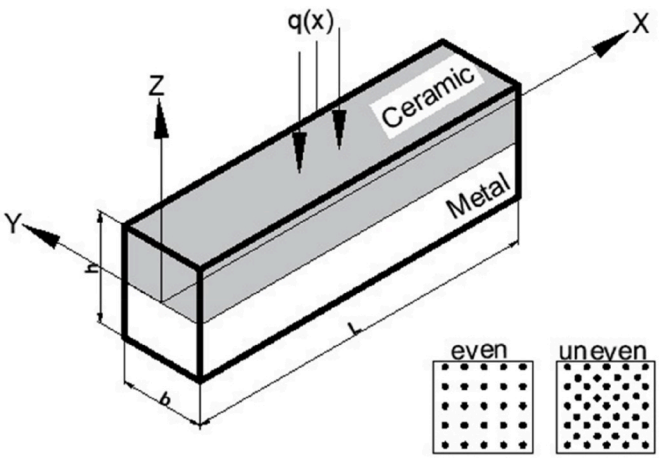

Fig. 1. BDFGPB geometry with even and uneven porosity.

linear elasticity. The selection of displacement fields for different shear deformation beam theories is predicated on certain assumptions. The axial as well as transverse displacements are divided into bending as well as shear components and the cross-sectional dimensions of the beam continue to be planar as well as perpendicular to the deformed axis after deformation. The transverse shear strain is considered to be constant across the thickness, and the shear deformation is assumed to be independent of the bending deformation. Assume linear elastic material behaviour, where the stress-strain relationship is attributed to being linear and Hooke's law is valid. Lastly, the shear component of the axial displacement results in higher-order fluctuations of shear strain, which consequently generates shear stress throughout the beam's depth. This shear stress is such that it disappears on the top and bottom surfaces.

The volume fraction (V_f) of BDFGPB is governed by power law, as given in Eq. (1), as stated in Ref. [56].

$$V_f(x,z) = \left(\frac{z}{h}+\frac{1}{2}\right)^{P_z}\left(\frac{x}{L}+\frac{1}{2}\right)^{P_x} \tag{1}$$

$$V_m + V_c = 1$$

where V_m, V_c are the volume fraction of the metal and ceramic, respectively.

The variables P_z and P_x represent the gradient index along the thickness (h) and length (L), respectively. At $P_x = 0$ and $P_z = 0$, the beam exhibits a homogeneous nature. The expression of material characteristics (F_a) that are beneficial in uniformly distributed BDFGPB can be represented as Eq. (2a), as stated in Ref. [57].

$$F(x,z) = (F_c - F_m)\left(\frac{z}{h}+\frac{1}{2}\right)^{P_z}\left(\frac{x}{L}+\frac{1}{2}\right)^{P_x} + F_m - \frac{\alpha}{2}(F_c + F_m) \tag{2a}$$

The symbol α denotes the porosity coefficient, which is constrained to the range of 0 – 0.4 [24]. The variables '*m*' and '*c*', respectively, refer to metal and ceramic materials. As per the above-mentioned correlation, the determination of material stiffness for uniformly distributed BDFGPB can be achieved through the utilization of the modulus of elasticity (E_a) and mass density (ρ_a) as presented in Eqs. (2b) and (2c).

$$E_a(x,z) = (E_c - E_m)\left(\frac{z}{h}+\frac{1}{2}\right)^{P_z}\left(\frac{x}{L}+\frac{1}{2}\right)^{P_x} + E_m - \frac{\alpha}{2}(E_c + E_m) \tag{2b}$$

$$\rho_a(x,z) = (\rho_c - \rho_m)\left(\frac{z}{h}+\frac{1}{2}\right)^{P_z}\left(\frac{x}{L}+\frac{1}{2}\right)^{P_x} + \rho_m - \frac{\alpha}{2}(\rho_c + \rho_m) \tag{2c}$$

Poisson's ratio (μ) is regarded as a constant due to the utilization of the mean value in calculations. Similarly, the characteristics of non-uniformly distributed BDFGPB can be approximated by utilizing Eq.

(2d):

$$F_a(x,z)=(F_c-F_m)\left(\frac{z}{h}+\frac{1}{2}\right)^{P_z}\left(\frac{x}{L}+\frac{1}{2}\right)^{P_x}+F_m-\frac{\alpha}{2}(F_c+F_m)\left(1-\frac{2|z|}{h}\right) \tag{2d}$$

E_a and ρ_a for unevenly distributed BDFGPB could be expressed in Eqs. (2e) and (2f):

$$E_a(x,z)=(E_c-E_m)\left(\frac{z}{h}+\frac{1}{2}\right)^{P_z}\left(\frac{x}{L}+\frac{1}{2}\right)^{P_x}+E_m-\frac{\alpha}{2}(E_c+E_m)\left(1-\frac{2|z|}{h}\right) \tag{2e}$$

$$\rho_a(x,z)=(\rho_c-\rho_m)\left(\frac{z}{h}+\frac{1}{2}\right)^{P_z}\left(\frac{x}{L}+\frac{1}{2}\right)^{P_x}+\rho_m-\frac{\alpha}{2}(\rho_c+\rho_m)\left(1-\frac{2|z|}{h}\right) \tag{2f}$$

2.2. Kinematics and constitutive equations

Structures composed of beams and plates made from FGM need to be carefully designed to ensure their durability and minimize production costs, especially when they are subjected to static and dynamic stresses. When analyzing these FGM structures using traditional beam and plate theories, it is often found that in most cases, the anticipated deflections are lower than what is really measured, whereas the natural frequencies are expected to be higher than they are. The displacement field for the BDFGPB adapting HSDT is shown in Eqs. (3a) and (3b), as stated in Ref. [56].

$$u(x,z)=u_0(x)+z\varnothing(x)-f(z)\left(\varnothing(x)+\frac{\partial w_0}{\partial x}(x)\right) \tag{3a}$$

$$w(x,z)=w_0(x) \tag{3b}$$

where " u" and " w" represent the axial and transverse displacements, respectively. At the given location on the neutral axis, u_0 and w_0 are the axial and transverse displacements, respectively. The partial derivative of w_0 with respect to x represents the bending slope, while $\varnothing$ denotes the shear slope. The present investigation considers the function $f(z)$ [58] as the shape function that governs the transverse shear deformation distribution, expressed in Eq. (4).

$$f(z)=\frac{4z^3}{3h^2} \tag{4}$$

The equations for computing the strain field (ε_x, γ_{xz}), which are non-zero, can be derived using the Eqs. (3a), (3b) and (4) are presented as Eqs. (5a) and (5b):

$$\varepsilon_x=\frac{\partial u}{\partial x}=\frac{\partial u_0}{\partial x}+\frac{\partial z}{\partial z}\varnothing-f(z)\left(\frac{\partial \varnothing}{\partial x}+\frac{\partial^2 w_0}{\partial x^2}\right) \tag{5a}$$

$$\gamma_{xz}=f'(z)\left[\varnothing+\frac{\partial w_0}{\partial x}\right] \tag{5b}$$

The stress field equations (σ_x, τ_{xz}) can be derived from Eq. (5a), and (5b) by applying Hooke's Law, as demonstrated in Eq. (6a), and (6b):

$$\sigma_x=\frac{E(x,z)}{1-\mu^2}\varepsilon_x \tag{6a}$$

$$\tau_{xz}=\frac{G(x,z)}{2(1+\mu)}\gamma_{xz} \tag{6b}$$

2.3. Governing equations of motion

One of the fundamental concepts in classical mechanics is the notion of least action. According to the Hamilton principle, the trajectory followed by a physical system between two places in configuration space is such that the action functional remains constant, as given in Eq. (7), as stated in Ref. [59].

$$\int_{t1}^{t2}(\delta U-\delta K)dt=0 \tag{7}$$

In which, time intervals are denoted as t_1 and t_2, while δU, and δK are changes in the potential energy, and the kinetic energy, respectively, while the change in potential energy in BDFGPB is given in Eq. (8a).

$$\delta U=\frac{1}{2}\int_0^L\int_{-\frac{h}{2}}^{+\frac{h}{2}}(\sigma_x\varepsilon_x+\tau_{xz}\gamma_{xz})dzdx \tag{8a}$$

substituting Eqs. (5a), (5b) and (6a), and (6b) into Eq. (8a), the potential energy could be deduced as,

$$\delta U=\int_0^L\int_{-\frac{h}{2}}^{+\frac{h}{2}}\left\{\sigma_x\left[\frac{du_o}{dx}+2\frac{d\varnothing}{dx}-f(z)\left(\frac{d\varnothing}{dx}+\frac{\partial^2 w_0}{\partial x^2}\right)\right]+\sigma_{xz}\left[\left(\frac{\partial w_0}{\partial x}+\varnothing-\frac{4z^2}{3h^2}\left(\varnothing+\frac{\partial w_0}{\partial x}\right)\right)\right]\right\}dzdx \tag{8b}$$

$$\delta U=\int_0^L\int_{-\frac{h}{2}}^{+\frac{h}{2}}\left\{\sigma_x\left[\frac{du_o}{dx}+2\frac{d\varnothing}{dx}-\frac{4z^2}{3h^2}\frac{d\varnothing}{dx}-\frac{4z^2}{3h^2}\frac{\partial^2 w_0}{\partial x^2}\right]+\sigma_{xz}\left[\left(\frac{\partial w_0}{\partial x}+\varnothing-\frac{4z^2}{h^2}\varnothing-\frac{4z^2}{h^2}\frac{\partial w_0}{\partial x}\right)\right]\right\}dzdx \tag{8c}$$

where, M_x, Q_x are the higher order terms in bending moment while, N_x, P_x, and R_x are the stress resultants.

$$M_x=\int_{-\frac{h}{2}}^{+\frac{h}{2}}z\sigma_x dz$$

$$P_x=\int_{-\frac{h}{2}}^{+\frac{h}{2}}z^3\sigma_x dz$$

$$N_x=\int_{-\frac{h}{2}}^{+\frac{h}{2}}\sigma_x dz$$

$$R_x=\int_{-\frac{h}{2}}^{+\frac{h}{2}}z^2\sigma_{xz}dz$$

$$Q_x=\int_{-\frac{h}{2}}^{+\frac{h}{2}}\sigma_{xz}dz$$

$$\delta U=\int_0^L\left[N_x\frac{du_0}{dx}+M_x\frac{d\varnothing}{dx}-\frac{4}{3h^2}P_x\frac{d\varnothing}{dx}-\frac{4}{3h^2}P_x\frac{d^2w_0}{dx^2}+Q_x\frac{dw_0}{dx}+Q_x\varnothing-\frac{4}{h^2}R_x\varnothing-\frac{4}{h^2}R_x\frac{dw_0}{dx}\right] \tag{8d}$$

The change in kinetic energy of a BDFGPB can be presented as,

$$\delta K = \frac{1}{2}\int_0^L \int_{-\frac{h}{2}}^{+\frac{h}{2}} \left[\left(\rho(\mathrm{x},z)E(\mathrm{x},\mathrm{z}) \left(I_0 \left(\frac{\partial u_0}{\partial z} \right)^2 - 2J_1 \frac{\partial u_0}{\partial t}\frac{d^2 w_0}{dxdz} + (2I_1 - 2J_1)\frac{\partial u_0}{\partial z}\frac{\partial \varnothing}{\partial z} + K_1 \left(\frac{d^2 w_0}{\partial xdz} \right)^2 + (2I_1 - 2I_1 J_1)\frac{d^2 w_0}{dxdz}\frac{\partial \varnothing}{\partial z} + (I_2 - 2I_1 J_1 + K_1)\left(\frac{\partial \varnothing}{\partial z} \right)^2 \right) \right) + \rho(\mathrm{x},z)E(\mathrm{x},\mathrm{z}) \left(\varnothing^2 (1 - 2I_2 + K_1) + \varnothing \frac{\partial w_0}{\partial z}(2 - 4I_2 - 2J_2) + \left(\frac{d^2 w_0}{dxdz} \right)^2 (1 - 2I_2 - J_2) \right) \right] dx \tag{9}$$

$$(\mathrm{I}_0, \mathrm{I}_1, \mathrm{I}_2, \mathrm{J}_1, \mathrm{J}_2, \mathrm{K}_1) = \int_{-\frac{h}{2}}^{+\frac{h}{2}} \left(1, \mathrm{z}, \mathrm{f}', \mathrm{f}, (\mathrm{f}')^2, (\mathrm{f})^2\right)$$

The mass inertias are denoted as $I_0, I_1, I_2, J_1, J_2, K_1$. The governing equations could be solved using KT conditions after functions $u_0(x,z)$, $w_0(x,z)$ and $\varnothing(x,z)$ having infinite dimensions are represented as generalized coordinates.

2.4. Kuhn-Tucker solution

The utilization of KT conditions in the study offers an optimization framework that enables the incorporation of constraints pertaining to material distribution, porosity, and finding the solutions for the governing equations. By taking into account the impact of limited optimization on the structural behavior, this strategy improves the precision of predictions especially in the considered beam model where the constraints are inequal. Assume that $f_k(x)$ $(k = 0, 1, 2, \ldots.. m)$ could be differentiated when the function $f_0(x)$ reaches to the point x^0, subjected to the given set $K = \left\{ \frac{x}{f_i(x)} \leq 0 (i = 1, 2, 3, \ldots\ldots.m) \right\}$ then the Lagrange multiplier, U^0 satisfies the following conditions for local minimum [60].

$$\frac{\partial f_0(x^0)}{\partial x_j} + \sum_{i=1}^{m} U_i^0 \frac{\partial f_0(x^0)}{\partial x_j} = 0 \ (j = 1, 2, 3, \ldots\ldots, n)$$

$$f_i(x^0) \leq 0 \ (i = 1, 2, 3, \ldots. m)$$

$$u_i^0 f_i(x^0) = 0 \ (i = 1, 2, 3, \ldots., m)$$

$$u_i^0 \geq 0 \ (i = 1, 2, 3, \ldots. m)$$

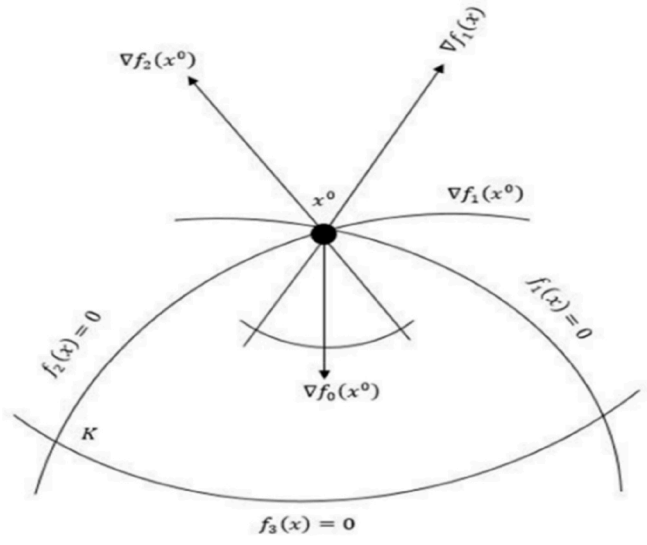

Fig. 2. KT condition.

Whereas, for maximization, the non-negativity condition $U^0 \leq 0$, are called the KT condition [60], as presented in Fig. 2.

$$L(x, z, u) = f_0(x) + \sum_{i=1}^{m} u_i \left(f_i(x) + z_i^2 \right)$$

The necessary condition for its local minimum is

$$\frac{\partial L}{\partial x_j} = \frac{\partial f_0(x^0)}{\partial x_j} + \sum_{i=1}^{m} u_i^0 \frac{\partial \left[f_i(x^0) + \left(z_i^0 \right)^2 \right]}{\partial x_j} = 0$$

$$\frac{\partial L}{\partial z_i} = 2u_i^0 z_i^0 = 0 \ (j = 1, 2, 3, \ldots. n)$$

$$\frac{\partial L}{\partial u_i} = f_i\left(x^0\right) + \left(z_i^0\right)^2 = 0 \ (i = 1, 2, 3, \ldots m)$$

$$\frac{\partial f_0[x^0(b)]}{\partial b_i} = -u_i^0 \ (i = 1, 2, 3, \ldots. m)$$

Without slack variables, the mathematical problem,

$$L(x, u) = f_0(x) + \sum\nolimits_{i=1}^{m} u_i f_i(x)$$

The KT condition can be rewritten as [60],

$$\frac{\partial L(x^0, u^0)}{\partial x_j} = 0 \ (j = 1, 2, 3, \ldots..n)$$

$$\frac{\partial L(x^0, u^0)}{\partial u_i} \leq 0 \ (i = 1, 2, 3, \ldots..m)$$

$$u_i^0 \frac{\partial L(x^0, u^0)}{\partial u_i} = 0 \ (i = 1, 2, 3, \ldots..m)$$

$$u_i^0 \geq 0 \ (i = 1, 2, 3, \ldots m)$$

If the multiplier u_i is positive, then the corresponding ith constraint is the boundary solution. When the function $u_0(x,z)$, $w_0(x,z)$ and $\varnothing_0(x,z)$ are expressed as generalized co-ordinates, it can be represented as Lagrange equations.

$$u_0(x, \mathrm{z}) = \sum_{i=1}^{m} f_i\left(x^0\right)\theta_i e^{i\lambda z} \tag{10}$$

$$w_0(x, z) = \sum_{i=1}^{m} f_i\left(x^0\right)\varphi_i e^{i\lambda z} \tag{11}$$

$$\varnothing_0(x, z) = \sum_{i=1}^{m} f_i\left(x^0\right)\psi_i e^{i\lambda z} \tag{12}$$

where, θ_i, φ_i, and ψ_i are the three different boundary conditions and λ is the scalar.

2.5. R-programming for KT conditions

The utilization of the R programming language facilitates the provision of comprehensive code documentation, promotes seamless cooperation, and enables the creation of user-friendly tools for subsequent applications. The R programming language is well recognized for its adaptability in managing mathematical and statistical calculations, rendering it highly suitable for the implementation of intricate analytical models and the execution of parametric investigations. By integrating R programming into the analysis of KT conditions [61], one can take advantage of R's robust mathematical libraries and data manipulation capabilities. Incorporating R into the process allows for the efficient computation of gradients, Hessians and constraint functions, which are crucial components of KT conditions. R's extensive package

ecosystem, including 'optim', 'nloptr', and 'quadprog', can be leveraged to find numerical solutions to optimization problems while adhering to KT conditions. This enables a thorough investigation into the impacts of several parameters, such as the distribution of materials and the level of porosity on the vibration properties. Furthermore, R's data visualization capabilities enable the effective representation of optimization results, aiding in the interpretation and decision-making process. By writing R scripts to handle KT conditions, practitioners gain a flexible and customizable approach to solving complex optimization problems with constraints. This integration not only streamlines the analysis but also provides a platform for analysis and model validation, ensuring the reliability and accuracy of optimization solutions in various real-world applications. R-program for KT boundary conditions are utilized for mathematical calculations as stated in Table 1.

From Table 1, the following conditions are formulated:

$$u_0(x,\mathrm{z}) = \sum_{i=1}^{m} f_i\left(x^0\right)\theta_i e^{i\omega z} \tag{13}$$

$$w_0(x,\mathrm{z}) = \sum_{i=1}^{m} f_i\left(x^0\right)\varphi_i e^{i\omega z} \tag{14}$$

$$\varnothing_0(x,\mathrm{z}) = \sum_{i=1}^{m} f_i\left(x^0\right)\psi_i e^{i\omega z} \tag{15}$$

where, θ_i, φ_i, and ψ_i are the three different boundary conditions and ω is the natural frequency. Substituting Eqs. (13)–(15) into Eqs. (8d) and (9), the equation of motion is derived and shown in Eq. (16).

$$\frac{\partial \mathrm{U}}{\partial \mathrm{f_j}} + \frac{\partial}{\mathrm{dt}}\left(\frac{\partial \mathrm{F}}{\partial \mathrm{f_j}}\right) = 0 \tag{16}$$

$$\left\{\begin{bmatrix} F_{11} & F_{12} & F_{13} \\ F_{21} & F_{22} & F_{23} \\ F_{31} & F_{32} & F_{33} \end{bmatrix} - \partial^2 \begin{bmatrix} N_{11} & N_{12} & N_{13} \\ N_{21} & N_{22} & N_{23} \\ N_{31} & N_{32} & N_{33} \end{bmatrix}\right\} \begin{bmatrix} X_1 \\ X_2 \\ X_3 \end{bmatrix} = \begin{bmatrix} 0 \\ 0 \\ 0 \end{bmatrix}$$

where $[F_{kl}]$ are the stiffness matrices and $[N_{kl}]$ are the mass matrices.

$$F_{11}(i,j) = X_1 \int_{-L/2}^{+L/2} e^{\omega x\left(\frac{x}{L}+\frac{1}{2}\right)} \theta_{i,j}\theta_{j,z}dx$$

$$F_{12}(i,j) = F_{21}(i,j) = -\alpha X_3 \int_{-L/2}^{+L/2} e^{\omega x\left(\frac{x}{L}+\frac{1}{2}\right)} \theta_{i,j}\varphi_{j,x}dx$$

$$F_{13}(i,j) = F_{31}(i,j) = (X_2 - \alpha X_1) \int_{-L/2}^{+L/2} e^{\omega x\left(\frac{x}{L}+\frac{1}{2}\right)} \theta_{i,j}\psi_{j,x}dx$$

$$F_{22}(i,j) = \alpha^2[K_{12}(i,j)][K_{13}(i,j)]$$

$$F_{23}(i,j) = F_{32}(i,j) = \left(\alpha^2 - \alpha F\right)[F_{22}(i,j)]$$

$$F_{33}(i,j) = \left(\alpha^2 - \alpha F\right)[F_{23}(i,j)]$$

Table 1
The boundary conditions based on the R-programming and KT conditions.

Demand/Boundary condition	$x = 0$	$x = L$
SS = q	$u = 0, w = 0$	$w = 0$
CC = z	$u = 0, w = 0, \varnothing = 0, w' = 0$	$u = 0, w = 0, \varnothing = 0, w' = 0$
CF = d	$u = 0, w = 0, \varnothing = 0, w' = 0$	–

$$N_{11}(i,j) = K_0 \int_{-L/2}^{+L/2} e^{\omega x\left(\frac{x}{L}+\frac{1}{2}\right)} \theta_i\theta_j dx$$

$$N_{12}(i,j) = N_{21}(i,j) = -\alpha K_1 \int_{-L/2}^{+L/2} e^{\omega x\left(\frac{x}{L}+\frac{1}{2}\right)} \theta_i\varphi_{j,x}dx$$

$$N_{13}(i,j) = N_{31}(i,j) = (K_0 - \alpha K_1) \int_{-L/2}^{+L/2} e^{\omega x\left(\frac{x}{L}+\frac{1}{2}\right)} \varphi_i\psi_j dx$$

$$N_{22}(i,j) = \left(\alpha^2 K_1 - \alpha K_1\right)[N_{11}(i,j)]$$

$$N_{23}(i,j) = N_{32}(i,j) = \left(\beta^2 K_0 - \alpha K_1\right)[N_{22}(i,j)]$$

$$N_{33}(i,j) = \left(K_2 + \alpha^2 K_1 - 2\alpha\beta\right)[N_{23}(i,j)]$$

where, i, j = 1, 2, 3, …. n

3. Results and discussion

3.1. The influence of P_x, and P_z on natural frequency of BDFGPB

A BDFGPB with a length that ranges from *0* to *L* and a thickness that ranges from *–h/2* to *+ h/2* is an example that is taken into consideration in order to evaluate the correctness of the suggested theory in terms of calculating natural frequencies and non-dimensional natural frequency (λ). Al/Al_2O_3 is the composition of the beam, and its characteristics are as follows: alumina has an E_c value of 380 GPa, a ρ_c value of 3960 kg/m^3 and a μ_c value of 0.3. On the other hand, aluminum has an E_m value of 70 GPa, a ρ_m value of 2702 kg/m^3, and a μ_m value of 0.3, as stated in Ref. [56]. By employing Equation (17) as stated in Ref. [58], it is possible to estimate a natural frequency (λ) that is also dimensionless.

$$\lambda = \frac{\omega L^2}{h}\sqrt{\frac{\rho_a}{E_a}} \tag{17}$$

where ω is the natural frequency.

The displacement functions with varied numbers of terms (m = 2, 4, 6, 8, 10 and 12) have been employed for the purposes of convergence and verification studies [58,62]. The results of the calculation are provided in the form of a dimensionless free vibration that takes into consideration gradient indices in both directions and boundary conditions. Studies conducted in the past by Reddy and Kumar [62] for dimensionless free vibration are used to compare the present results and summarized in Tables 2–4 for the SS, CC and CF boundary conditions, respectively, at L/h = 5. The λ of SS, CC and CF beams converged at the 4th term, but the results were evaluated up to the 12th term. Reddy and Kumar [62] have used the two directional functionally graded porous beam to analyze the free vibrations by applying HSDT and adapting Lagrange's method and Navier's method in solving the governing equations. In Tables 2–4, the natural frequencies of the BDFGPB did not converge at the 2nd term. Instead, it happened from the 4th term with the use of KT conditions and the R program further the calculations are done up to the 2nd term while the results in Reddy and Kumar [62] converged in the 6th and 8th term. This can be attributed to the complexity of the problem and the need for higher-order terms to accurately capture the behaviour of the system. In the analysis of composite structures like FGBs, higher-order terms are often required to account for material gradients, boundary conditions as well as geometric properties. The second-term approximation may not capture all the gradations of the system, leading to discrepancies in the predicted natural frequencies. BDFGPB with larger gradation exponents have, on average, more natural frequencies than FGBs with smaller gradation exponents. In contrast, a beam with a lower gradation exponent is less

Table 2
The influence of P_x, and P_z, on λ for a SS BDFGPB at L/h = 5.

Beam Theory		P_x	P_z						
			0	0.1	0.3	0.5	0.7	0.9	1
[62]		0	3.218	3.212	3.202	3.186	3.165	3.154	3.379
Present	2 terms		3.481	3.452	3.395	3.388	3.373	3.367	3.337
	4 terms		3.343	3.319	3.307	3.291	3.273	3.261	3.253
	6 terms		3.343	3.319	3.307	3.291	3.273	3.261	3.253
	8 terms		3.343	3.319	3.307	3.291	3.273	3.261	3.253
	10 terms		3.343	3.319	3.307	3.291	3.273	3.261	3.253
	12 terms		3.343	3.319	3.307	3.291	3.273	3.261	3.253
[62]		0.5	3.213	3.208	3.197	3.180	3.159	3.148	3.375
Present	2 terms		3.476	3.448	3.392	3.382	3.367	3.36	3.329
	4 terms		3.338	3.315	3.304	3.285	3.267	3.254	3.245
	6 terms		3.338	3.315	3.304	3.285	3.267	3.254	3.245
	8 terms		3.338	3.315	3.304	3.285	3.267	3.254	3.245
	10 terms		3.338	3.315	3.304	3.285	3.267	3.254	3.245
	12 terms		3.338	3.315	3.304	3.285	3.267	3.254	3.245
[62]		1.0	3.185	3.180	3.169	3.154	3.133	3.121	3.351
Present	2 terms		3.026	2.985	2.947	2.893	2.862	2.819	2.776
	4 terms		2.888	2.847	2.809	2.755	2.724	2.681	2.638
	6 terms		2.888	2.847	2.809	2.755	2.724	2.681	2.638
	8 terms		2.888	2.847	2.809	2.755	2.724	2.681	2.638
	10 terms		2.888	2.847	2.809	2.755	2.724	2.681	2.638
	12 terms		2.888	2.847	2.809	2.755	2.724	2.681	2.638

Table 3
The influence of P_x, and P_z, on λ for a CC BDFGPB at L/h = 5.

Beam Theory		P_x	P_z						
			0	0.1	0.3	0.5	0.7	0.9	1
[62]		0	6.243	6.242	6.236	6.224	6.205	6.180	6.166
Present	2 terms		6.222	6.221	6.215	6.202	6.184	6.159	6.145
	4 terms		6.179	6.178	6.172	6.160	6.141	6.117	6.103
	6 terms		6.179	6.178	6.172	6.160	6.141	6.117	6.103
	8 terms		6.179	6.178	6.172	6.160	6.141	6.117	6.103
	10 terms		6.179	6.178	6.172	6.160	6.141	6.117	6.103
	12 terms		6.179	6.178	6.172	6.160	6.141	6.117	6.103
[62]		0.5	6.248	6.247	6.241	6.231	6.213	6.185	6.171
Present	2 terms		6.215	6.214	6.208	6.195	6.177	6.152	6.138
	4 terms		6.172	6.171	6.165	6.153	6.134	6.11	6.096
	6 terms		6.172	6.171	6.165	6.153	6.134	6.11	6.096
	8 terms		6.172	6.171	6.165	6.153	6.134	6.11	6.096
	10 terms		6.172	6.171	6.165	6.153	6.134	6.11	6.096
	12 terms		6.172	6.171	6.165	6.153	6.134	6.11	6.096
[62]		1.0	6.273	6.272	6.266	6.254	6.235	6.21	6.196
Present	2 terms		6.211	6.21	6.204	6.191	6.173	6.148	6.134
	4 terms		6.168	6.167	6.161	6.149	6.130	6.106	6.092
	6 terms		6.168	6.167	6.161	6.149	6.130	6.106	6.092
	8 terms		6.168	6.167	6.161	6.149	6.130	6.106	6.092
	10 terms		6.168	6.167	6.161	6.149	6.130	6.106	6.092
	12 terms		6.168	6.167	6.161	6.149	6.130	6.106	6.092

rigid, resulting in a reduced natural frequency. According to the power law, greater values of gradation exponents result in a greater power of z/L, causing a more rapid modification of the material's characteristics along the length and thickness axes.

3.2. The influence of P_x, and P_z on the frequency of natural phenomenon

The gradient index effect is influential because the free vibration decreases as the gradient index increases (Figs. 3–5). Material and cross-sectional shape affect the beam stiffness under SS boundary conditions as can be seen in Fig. 3. It is observed from Fig. 3 that, at L/h = 5, the values of λ for $P_z = 0.1$, at $P_x = 0.1$, 0.3, 0.5, 0.7 and 0.9 were found to be 2.294, 2.260, 2.241, 2.231 and 2.226 respectively. Whereas at $P_z = 0.7$, at $P_x = 0.1$, 0.3, 0.5, 0.7 and 0.9 were found to be 2.222, 2.188, 2.171, 2.162 and 2.131 respectively. On the other hand, at L/h = 5 and $P_x = 0.2$, the values of λ for $P_z = 0.1$, 0.3, 0.5, 0.7, 0.9 were found to be 2.277, 2.253, 2.229, 2.215, 2.211 respectively and at $P_x = 0.8$, the values of λ for $P_z = 0.1$, 0.3, 0.5, 0.7, 0.9 were found to be 2.267, 2.244, 2.220, 2.206, 2.202 respectively. The gradient index effect is influential because the free vibration decreases as the gradient index increases. A similar trend was observed in Karamanli [58] and Reddy and Kumar [62].

Fig. 4 depicts material and cross-sectional shape affect the beam stiffness under CC boundary conditions. It is observed from Fig. 4 that, at L/h = 5, the values of λ for $P_z = 0.1$, at $P_x = 0.1$, 0.3, 0.5, 0.7 and 0.9 were found to be 4.116, 3.994, 3.872, 3.793 and 3.682 respectively. Whereas at $P_z = 0.7$, at $P_x = 0.1$, 0.3, 0.5, 0.7 and 0.9 were found to be 4.099, 3.987, 3.856, 3.777 and 3.667 respectively. On the other hand, at L/h = 5 and $P_x = 0.2$, the values of λ for $P_z = 0.1$, 0.3, 0.5, 0.7, 0.9 were found to be 4.086, 4.078, 4.058, 4.034 and 4.006 respectively. It can be inferred that the change in the volume fraction could result in a greater variation in the elastic modulus along the length which enhances the beam's overall stiffness and consequently, its natural frequency. Increasing the gradient index for a CC boundary condition can decrease stiffness. The impact of the gradient index on the natural frequency of a

Table 4
The influence of P_x, and P_z, on λ for a CF BDFGPB at L/h = 5.

Beam Theory		P_x	P_z						
			0	0.1	0.3	0.5	0.7	0.9	1
[62]		0	1.286	1.286	1.284	1.280	1.275	1.268	1.264
Present	2 terms		1.252	1.251	1.25	1.246	1.241	1.234	1.230
	4 terms		1.184	1.184	1.182	1.178	1.173	1.166	1.162
	6 terms		1.184	1.184	1.182	1.178	1.173	1.166	1.162
	8 terms		1.184	1.184	1.182	1.178	1.173	1.166	1.162
	10 terms		1.184	1.184	1.182	1.178	1.173	1.166	1.162
	12 terms		1.184	1.184	1.182	1.178	1.173	1.166	1.162
[62]		0.5	1.172	1.172	1.170	1.166	1.158	1.151	1.150
Present	2 terms		1.160	1.160	1.159	1.155	1.147	1.14	1.139
	4 terms		1.138	1.138	1.136	1.133	1.125	1.118	1.117
	6 terms		1.138	1.138	1.136	1.133	1.125	1.118	1.117
	8 terms		1.138	1.138	1.136	1.133	1.125	1.118	1.117
	10 terms		1.138	1.138	1.136	1.133	1.125	1.118	1.117
	12 terms		1.138	1.138	1.136	1.133	1.125	1.118	1.117
[62]		1	1.024	1.024	1.022	1.019	1.015	1.010	1.007
Present	2 terms		1.007	1.007	1.006	1.003	0.999	0.994	0.991
	4 terms		0.975	0.975	0.974	0.971	0.967	0.962	0.959
	6 terms		0.975	0.975	0.974	0.971	0.967	0.962	0.959
	8 terms		0.975	0.975	0.974	0.971	0.967	0.962	0.959
	10 terms		0.975	0.975	0.974	0.971	0.967	0.962	0.959
	12 terms		0.975	0.975	0.974	0.971	0.967	0.962	0.959

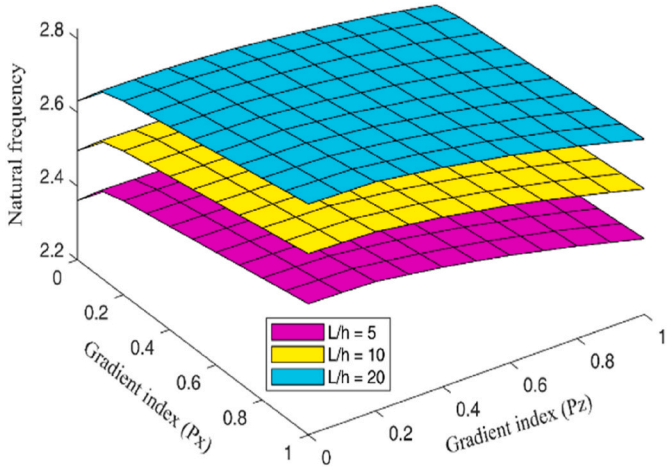

Fig. 3. Variation in λ of SS beam with respect to aspect ratios along P_x and P_z

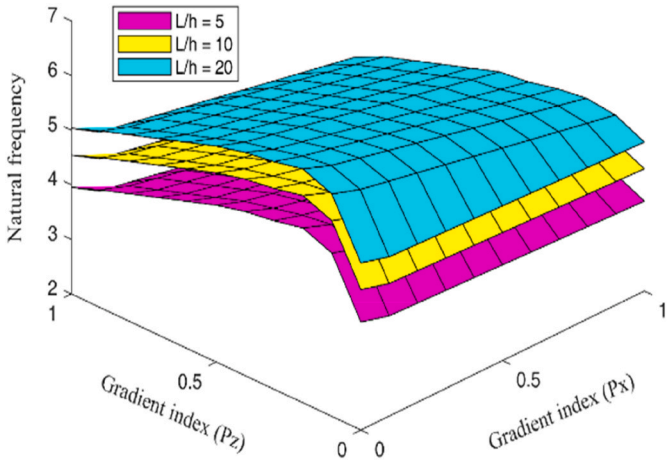

Fig. 4. Variation in λ of CC beam with respect to aspect ratios along P_x and P_z

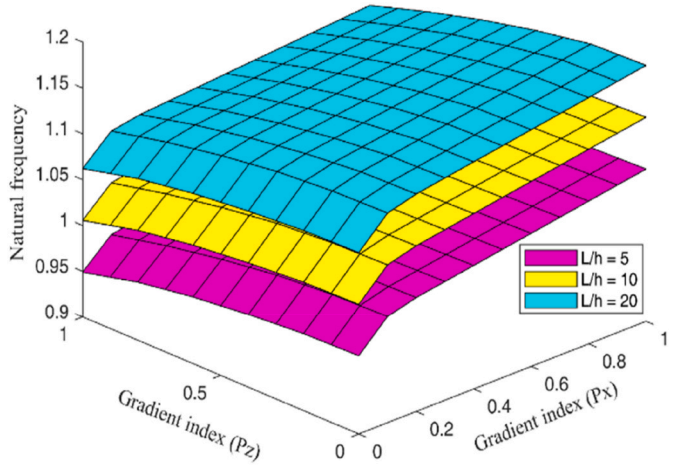

Fig. 5. Variation in λ of CF beam with respect to aspect ratios along P_x and P_z

CF BDFGPB (Fig. 5.) is distinct from that of CC and SS boundary conditions. As the displacement at the free end is not present, the rigidity of a CF beam is independent of changes in the volume fraction of solid material near the free end. Consequently, the gradient index exerts less influence on the natural frequency of a CF BDFGPB as compared with the SS and CC BDFGPBs.

The *x*-direction gradient index signifies a variation in material characteristics throughout the beam's length. A rise in the gradient index along the *x*-direction indicates a greater degree of variation in the qualities of the material. Greater variations in material properties might result in enhanced flexibility or reduced stiffness along the *x*-direction. A drop in natural frequency is observed as a consequence of reduced stiffness. Consequently, the beam exhibits more flexibility and vibrates at reduced frequencies and this could be advantageous in situations where there is a need for vibration control or dampening. The variation in material properties throughout the height of the beam is shown by the gradient index in the *z*-direction. An augmentation in the gradient index along the *z*-direction signifies a heightened degree of vertical variation in material properties. The observed variability has the potential to impact the dispersion of shear forces and bending moments inside the beam, hence exerting an influence on its composite stiffness. Analogous to the *x*-direction, an augmentation in flexibility or a diminution in

rigidity in the z-direction might result in a decline in the natural frequency. This trend applies to designs that require vertical flexibility or aim to decrease vibration.

Eq. (17) suggests that the λ is influenced by the system's parameters such as ω, L, h, ρ_a and E_a. P_z and P_x are the gradient indices that control the spatial variation of material properties along the x and z directions. The effect of variations in material properties can be indirectly assessed by examining their influence on the overall response of the beam as presented in Eqs. (2b), (2c), (2e) and (2f). Higher gradient indices, in both the x and z directions, have the potential to affect the configuration of stiffness as well as mass inside the beam, hence influencing its natural frequency and dynamic characteristics in such a way that the natural frequency decreases with an increase in the gradient index in both directions. Moreover, a higher natural frequency or larger characteristic length tends to increase the λ, while a larger thickness, mass density or Young's modulus tends to decrease the λ.

3.3. The influence of porosity on the frequency of natural phenomenon

Table 5 and Figs. 6–8 show the natural frequency changes in a BDFGPB with porosity for SS, CC and CF beams. The porosity and porosity index influence the material gradation and subsequently the non-dimensional natural frequency. The latter finding is in good agreement with the fact that typically, the natural frequency of a BDFGPB increases as its porosity increases. Because of the presence of pores, the material's rigidity and density decrease, and the beam's resistance to deformation and oscillation is also affected. For instance, an increase in the porosity index results in a more uniform distribution of rigidity and mass, subsequently it leads to a higher natural frequency. Even the distribution of porosity within BDFGPB results in greater homogeneity in the distribution of mass and rigidity, which could lead to a higher natural frequency. A more homogenous distribution of mass and rigidity increases the likelihood of local stress concentrations and decreases the beam's resistance to deformation and oscillation [64]. Alternatively, an uneven porosity in a BDFGPB may lead to an uneven distribution of mass and rigidity, which will decrease the natural frequency. The non-uniform distribution of mass and rigidity can contribute to the concentration of tension in specific regions, resulting in a lesser stiffness and, consequently, a lesser natural frequency.

As depicted in Fig. 6(a) and (b), the effect of uniform porosity on the natural frequency of an SS BDFGPB is significant. Specifically, the natural frequency decreases as the gradient index in the material increases. Because of this, the porosity reduces the effective rigidity, resulting in a lower natural frequency, while the even porosity can influence the beam's mode configurations. It can be seen from Fig. 6(a) that the even porosity may lead the mode forms to be symmetric about the axis of the beam cross-section. This can have significant repercussions for the structure of the beam. The even porosity of this beam has the potential to influence the proportions of aluminium as well as alumina, and that in turn has the potential to change the effective stiffness along with mass of the beam. In addition, the inclusion of alumina in the BDFGPB might result in the introduction of extra stiffness as well as mass effects. This is because alumina has a naturally high density as well as stiffness. From Table 5, under even porosity of an SS beam (Fig. 6(b)), at $\alpha = 0.1$, $P_z = 2$ and $P_x = 2$, $\lambda = 2.0673$ whereas, under uneven porosity conditions, at $\alpha = 0.1$, $P_z = 2$, $P_x = 2$, $\lambda = 2.0440$. This shows a decrease in natural frequency under uneven porosity distribution as compared with even porosity distribution for the same gradient index value. Uneven distribution of porosity, on the other hand, can also result in a non-uniform distribution of alumina throughout the beam. This, in turn, can have an additional impact on the effective stiffness as well as the mass of the beam in particular locations [65]. It can be observed from Table 5 that for an SS beam under even porosity, at $\alpha = 0.2$, $P_x = 4$, $P_z = 4$, $\lambda = 1.7919$ whereas, $\alpha = 0.3$, $P_x = 10$, $P_z = 10$, then $\lambda = 1.4418$. Additionally, the uneven distribution of porosity, as well as, alumina could also lead to non-symmetric mode forms of the beam, which could make the BDFGPB structural response to dynamic loading more complicated.

In contrast to an SS beam, the boundary constraints of the CC enforce a set limit at each end of the beam, which might lead to differences in the mode shapes as well as natural frequencies that are manifested in Fig. 7 (a) and (b). SS beams usually vibrate at their supports, which suggests that the support points might cause maximum displacement and minimal bending moment, resulting in a beam with reduced effective stiffness, which in turn lowers natural frequency [63]. On the contrary, CC beams are stationary at both ends, which shows that the beam's center vibrates rather than the support points being fixed. Fixed boundary conditions improve the beam's natural frequency and effective stiffness [64]. In addition, the beam's mode forms might change across boundary circumstances. The mode shapes of CC beams have the greatest amplitude near the beam's center.

The difference among different types of porosity distribution may grow more obvious with an increase in the porosity index (α). This infers that the porosity in the direction of thickness (z) has a larger effect on vibration than that in the axial direction (x). BDFGPB with an even porosity distribution experience free vibration more frequently than those with an asymmetrical porosity distribution [65]. The value of a CF beam's free vibration decreases as the gradation exponents in the x and z directions increase and increases as the porosity index increases as

Table 5
The effect of α on λ for SS, CC, and CF BDFGPB at aspect ratio L/h = 5.

Boundary Condition	P_x & P_z	Even Porosity with porosity coefficient				Uneven Porosity with porosity coefficient			
		0	0.1	0.2	0.3	0	0.1	0.2	0.3
SS	0	5.1532	5.2202	5.3021	5.4013	5.1532	5.2202	5.3021	5.4013
	2	2.0408	2.0673	2.0998	2.1391	2.0408	2.0440	2.0483	2.0532
	4	1.7416	1.7642	1.7919	1.8254	1.7416	1.7443	1.7480	1.7522
	6	1.5486	1.5687	1.5934	1.6232	1.5486	1.5510	1.5543	1.5580
	8	1.4622	1.4812	1.5045	1.5326	1.4622	1.4645	1.4676	1.4711
	10	1.3756	1.3935	1.4154	1.4418	1.3756	1.3777	1.3807	1.3840
CC	0	10.0321	10.1620	10.3224	10.5154	10.0321	10.1620	10.3224	10.5154
	2	4.2677	4.3230	4.3912	4.4733	4.2677	4.2859	4.3080	4.3318
	4	3.3517	3.3951	3.4487	3.5132	3.3517	3.3660	3.3833	3.4021
	6	2.7647	2.8005	2.8447	2.8979	2.7647	2.7765	2.7908	2.8062
	8	2.5067	2.5392	2.5792	2.6275	2.5067	2.5174	2.5304	2.5444
	10	2.2395	2.2685	2.3043	2.3474	2.2395	2.2490	2.2606	2.2731
CF	0	1.8948	1.9202	1.9505	1.9869	1.8948	1.9202	1.9505	1.9869
	2	0.7696	0.7799	0.7922	0.8070	0.7696	0.7706	0.7718	0.7729
	4	0.6716	0.6806	0.6913	0.7043	0.6716	0.6725	0.6735	0.6745
	6	0.6060	0.6141	0.6238	0.6355	0.6060	0.6068	0.6077	0.6086
	8	0.5732	0.5809	0.5900	0.6011	0.5732	0.5739	0.5748	0.5757
	10	0.5408	0.5480	0.5567	0.5671	0.5408	0.5415	0.5423	0.5431

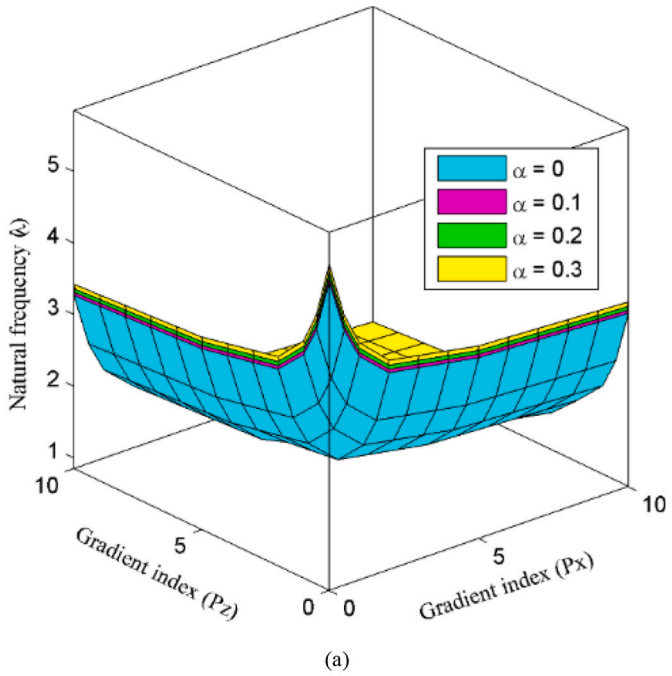

Fig. 6. Effect of α on λ for SS BDFGPB with even (a) and uneven (b) porosity at aspect ratio L/h = 5.

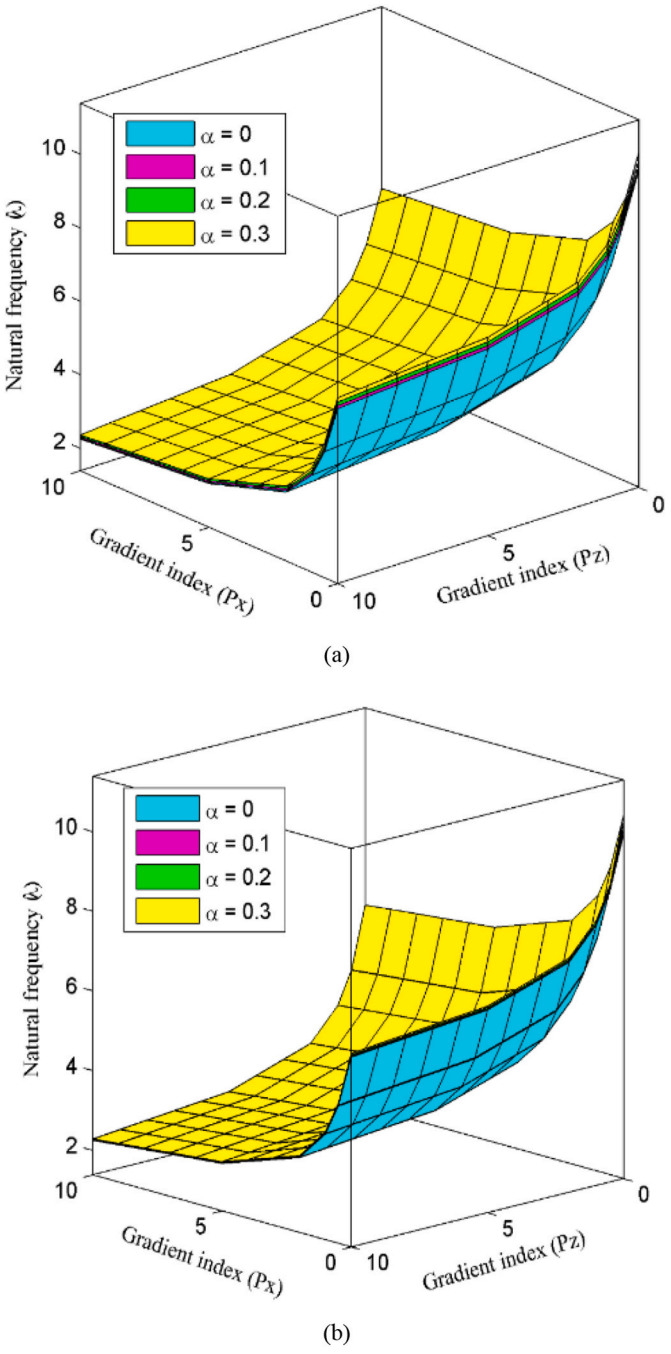

Fig. 7. Effect of α on λ for CC BDFGPB with even (a) and uneven (b) porosity at aspect ratio L/h = 5.

shown in Fig. 8(a) and (b). This is because, as the value of porosity increases, the flexible rigidity of the beam decreases [59]. When the gradient index equals zero, a beam is deemed to be made of pure metal, and its rigidity is diminished [66]. As the gradient index approaches infinity, a beam approaches the rigidity of pure ceramic, which reduces vibration.

4. Conclusion

The current study focused on the analysis of the free vibration behavior of BDFGPB, considering different boundary conditions, namely simply supported, clamped-clamped and clamped-free. The following are the most notable findings:

- The beam theory utilized in this study to resolve the free vibration responses of the BDFGPB ensures that the top and bottom surfaces of the beam satisfy the zero traction boundary conditions.
- As compared with the existing solution methods, the novel application of KT conditions method using R-program in this computational method proves its adaptability and that the results of the non-dimensional natural frequency are found to be converged at 4th term.
- In comparison to the reference study, the non-dimensional natural frequencies for the SS, CC, and CF boundary conditions deviated by 3.19%, 1.25%, and 2.15%, respectively, at $P_x = 0.5$ and $P_z = 0.5$
- The dimensionless natural frequency for the CC boundary condition is highest followed by SS and CF. When switching from CC to merely

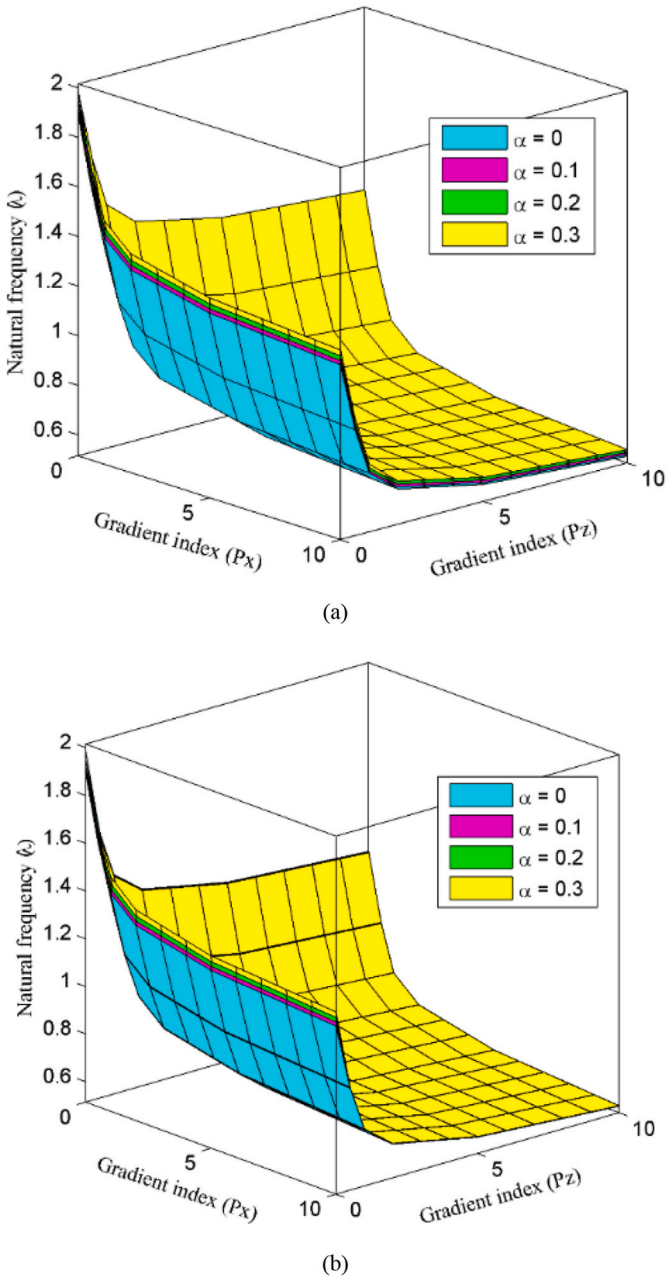

Fig. 8. Effect of α on λ for CF BDFGPB with even (a) and uneven (b) porosity at aspect ratio L/h = 5.

SS and CF boundary conditions, the dimensionless natural frequency decreases and the drop reflects a decrease in beam stiffness and rigidity.

- Gradient indices strongly affect the dimensionless natural frequency of the BDFGPB. The dimensionless natural frequency decreases as P_x and P_z increases. Variations in the beam's stiffness and subsequent effects on its vibration characteristics are influenced by different values of the gradient indices and boundary conditions.
- The influence of porosity on the dimensional natural frequency of even and uneven BDFGPB can vary based on the boundary conditions.
- As the porosity index increases, both even and uneven porosity conditions result in an increase in the dimensionless natural frequency of the BDFGPB for SS, CC and CF boundary conditions.

Porosity is an essential factor in modern structure design, affecting efficacy and responsiveness. Understanding how porosity impacts the natural frequency of a beam is crucial for optimizing its behavior. Therefore, to predict this, both porosity distribution and material properties must be considered. The discussion presented in this study will serve as a benchmark result for studying bi-directionally functionally graded porous beams subjected to thermal stresses, showing agreement with prior research and validating the beam model.

CRediT authorship contribution statement

Geetha Narayanan Kannaiyan: Writing – original draft, Formal analysis, Conceptualization. **Vivekanandam Balasubramaniam:** Validation, Methodology, Formal analysis. **Bridjesh Pappula:** Validation, Supervision, Data curation. **Seshibe Makgato:** Writing – review & editing, Supervision.

Declaration of competing interest

The authors declare that they have no known competing financial interests or personal relationships that could have appeared to influence the work reported in this paper.

Data availability

No data was used for the research described in the article.

References

[1] Y. Miyamoto, W.A. Kaysser, B.H. Rabin, A. Kawasaki, R.G. Ford, Processing and fabrication, in: Functionally Graded Materials, Springer, Boston, MA, 1999.
[2] S.O.W. Khafaji, M.A. Al-Shujairi, M.J. Aubad, Transient analysis of transversely functionally graded Timoshenko beam (TFGTB) in conjunction with finite element method, Arch. Mech. Eng. 67 (2020) 299–321.
[3] B. Kılıç, Ö. Özdemir, Vibration and stability analyses of functionally graded beams, Arch. Mech. Eng. 68 (2021) 93–113.
[4] J.E. Jam, M. Noorabadi, N. Namdaran, Nonlinear free vibration analysis of micro-beams resting on viscoelastic foundation based on the modified couple stress theory, Arch. Mech. Eng. 64 (2017) 239–256.
[5] T.Q. Hung, T.M. Tu, D.M. Duc, Free vibration analysis of sandwich beam with porous FGM core in thermal environment using mesh-free approach, Arch. Mech. Eng. 69 (2022) 471–496.
[6] A. Salman, N. Al-Ghaban, M. Eesa, A. Atiyah, S. Farid, Osseointegration of cylindrical Zirconia–alumina functionally graded materials, dental implant by Electrophoretic Deposition, Ziggurat Journal of Materials Technology 1 (2020) 2–12.
[7] S. Rouf, A. Malik, A. Raina, M.I. Haq, N. Naveed, A. Zolfagharian, M. Bodaghi, Functionally graded additive manufacturing for orthopedic applications, J. Orthop. 33 (2022) 70–80.
[8] I.M. Nazmul, S. Nahid, D. Indronil, Analytical solutions for vibration of Bi-directional functionally graded nonlocal nanobeams, Results in Engineering 18 (2023) 101046.
[9] A. Kalhori, M.J. Bayat, K. Asemi, Buckling analysis of stiffened functionally graded multilayer graphene platelet reinforced composite plate with circular cutout embedded on elastic support subjected to in-plane normal and shear loads, Results in Engineering 20 (2023) 101563.
[10] T.H. Nguyen, T.T. Nguyen, T.T. Tran, Q.H. Pham, Research on the mechanical behaviour of functionally graded porous sandwich plates using a new C1 finite element procedure, Results in Engineering 17 (2023) 100817.
[11] A. Jarrahi, H.A. Shirazi, A. Asnafi, M.R. Ayatollahi, Biomechanical analysis of a radial functionally graded dental implant–bone system under multi-directional dynamic loads, J. Braz. Soc. Mech. Sci. Eng. 40 (2018) 1–3.
[12] Y. Tang, J.Y. Xu, L.Q. Chen, T. Yang, Nonlinear dynamics of an enhanced piezoelectric energy harvester composited of bi-directional functional graded materials, Int. J. Non Lin. Mech. 150 (2023) 104350.
[13] H. Qing, L. Wei, Linear and nonlinear free vibration analysis of functionally graded porous nanobeam using stress-driven nonlocal integral model, Communications in Nonlinear Science and Numerical Simulation 109 (2022) 106300.
[14] N.D. Nguyen, T.N. Nguyen, T.K. Nguyen, T.P. Vo, A new two-variable shear deformation theory for bending, free vibration and buckling analysis of functionally graded porous beams, Compos. Struct. 282 (2022) 115095.
[15] T.Q. Hung, D.M. Duc, T.M. Tu, Free and forced vibration characteristics of functionally graded sandwich beam with GPL-reinforced porous core, in: Proceedings of the 17th East Asian-Pacific Conference on Structural Engineering and Construction, 2022: EASEC-17, Singapore, Springer Nature Singapore, Singapore, 2023, pp. 1432–1452.
[16] S. Refrafi, A.A. Bousahla, A. Bouhadra, A. Menasria, F. Bourada, A. Tounsi, E. A. Bedia, S.R. Mahmoud, K.H. Benrahou, A. Tounsi, Effects of hygro-thermo-

mechanical conditions on the buckling of FG sandwich plates resting on elastic foundations. Computers and Concrete, Int. J. 25 (2020) 311–325.
[17] I.M. Mudhaffar, A. Tounsi, A. Chikh, M.A. Al-Osta, M.M. Al-Zahrani, S.U. Al-Dulaijan, Hygro-thermo-mechanical bending behavior of advanced functionally graded ceramic metal plate resting on a viscoelastic foundation, Structures 33 (2021) 2177–2189.
[18] J. Zhao, Q. Wang, X. Deng, K. Choe, F. Xie, C. Shuai, A modified series solution for free vibration analyses of moderately thick functionally graded porous (FGP) deep curved and straight beams, Compos. B Eng. 165 (2019) 155–166.
[19] P. Van Vinh, A. Tounsi, M.O. Belarbi, On the nonlocal free vibration analysis of functionally graded porous doubly curved shallow nanoshells with variable nonlocal parameters, Eng. Comput. 39 (2023) 835–855.
[20] M. Arefi, M. Meskini, Application of hyperbolic shear deformation theory to free vibration analysis of functionally graded porous plate with piezoelectric face-sheets, Structural Engineering and Mechanic 71 (2019) 459–467.
[21] S.K. Jena, S. Chakraverty, V. Mahesh, D. Harursampath, Application of Haar wavelet discretization and differential quadrature methods for free vibration of functionally graded micro-beam with porosity using modified couple stress theory, Eng. Anal. Bound. Elem. 140 (2022) 167–185.
[22] H. Salehipour, D. Shahgholian-Ghahfarokhi, A. Shahsavar, O. Civalek, M. Edalati, Static deflection and free vibration analysis of functionally graded and porous cylindrical micro/nano shells based on the three-dimensional elasticity and modified couple stress theories, Mech. Base. Des. Struct. Mach. 50 (6) (2022) 2184–2205, 2022.
[23] K. Gao, R. Li, J. Yang, Dynamic characteristics of functionally graded porous beams with interval material properties, Eng. Struct. 197 (2019) 109441.
[24] N.T.B. Phuong, T.M. Tu, H.T. Phuong, N. Van Long, Bending analysis of functionally graded beam with porosities resting on elastic foundation based on neutral surface position, Journal of Science and Technology in Civil Engineering (STCE)-HUCE 13 (2019) 33–45.
[25] T. Quang Hung, D.M. Duc, T. Minh Tu, Static bending mesh-free analysis of smart piezoelectric porous beam reinforced with graphene platelets, Proc. IME C J. Mech. Eng. Sci. 237 (2023) 1595–1612.
[26] C.W. Lim, G. Zhang, J. Reddy, A higher-order nonlocal elasticity and strain gradient theory and its applications in wave propagation, J. Mech. Phys. Solid. 78 (2015) 298–313.
[27] F. Ebrahimi, M.R. Barati, Hygrothermal effects on vibration characteristics of viscoelastic FG nanobeams based on nonlocal strain gradient theory, Compos. Struct. 159 (2017) 433–444.
[28] S. Sahmani, M.M. Aghdam, Nonlocal strain gradient beam model for nonlinear vibration of prebuckled and postbuckled multilayer functionally graded GPLRC nanobeams, Compos. Struct. 179 (2017) 77–88.
[29] G.L. She, F.G. Yuan, Y.R. Ren, H.B. Liu, W.S. Xiao, Nonlinear bending and vibration analysis of functionally graded porous tubes via a nonlocal strain gradient theory, Compos. Struct. 203 (2018) 614–623.
[30] Y. Gao, W. Xiao, H. Zhu, Nonlinear vibration of functionally graded nano-tubes using nonlocal strain gradient theory and a two-steps perturbation method, Struct. Eng. Mech. 69 (2019) 205–219.
[31] M.H. Ghazwani, A. Alnujaie, M. Avcar, P. Van Vinh, Examination of the high-frequency behavior of functionally graded porous nanobeams using nonlocal simple higher-order shear deformation theory, Acta Mech. (2024), https://doi.org/10.1007/s00707-024-03858-6.
[32] F. Mellal, R. Bennai, M. Avcar, M. Nebab, H.A. Atmane, On the vibration and buckling behaviors of porous FG beams resting on variable elastic foundation utilizing higher-order shear deformation theory, Acta Mech. 234 (2023) 3955–3977.
[33] M. Avcar, L. Hadji, R. Akan, The influence of Winkler-Pasternak elastic foundations on the natural frequencies of imperfect functionally graded sandwich beams, Geomechanics and Engineering 31 (1) (2022) 99–112.
[34] L. Hadji, M. Avcar, Nonlocal free vibration analysis of porous FG nanobeams using hyperbolic shear deformation beam theory, Advances in Nano Research 10 (3) (2021) 281–293.
[35] M. Al-Shujairi, C. Mollamahmutoğlu, Dynamic stability of sandwich functionally graded micro-beam based on the nonlocal strain gradient theory with thermal effect, Compos. Struct. 201 (2018) 1018–1030.
[36] H. Liu, Z. Lv, H. Wu, Nonlinear free vibration of geometrically imperfect functionally graded sandwich nanobeams based on nonlocal strain gradient theory, Compos. Struct. 214 (2019) 47–61.
[37] S. Guo, Y. He, D. Liu, J. Lei, Z. Li, Dynamic transverse vibration characteristics and vibro-buckling analyses of axially moving and rotating nanobeams based on nonlocal strain gradient theory, Microsyst. Technol. 24 (2018) 963–977.
[38] L. Lu, X. Guo, J. Zhao, A unified size-dependent plate model based on nonlocal strain gradient theory including surface effects, Appl. Math. Model. 68 (2019) 583–602.
[39] M. Mohammadian, M.H. Abolbashari, S.M. Hosseini, Application of hetero junction CNTs as mass nanosensor using nonlocal strain gradient theory: an analytical solution, Appl. Math. Model. 76 (2019) 26–49.
[40] B. Karami, M. Janghorban, T. Rabczuk, Dynamics of two-dimensional functionally graded tapered Timoshenko nanobeam in thermal environment using nonlocal strain gradient theory, Compos. B Eng. 182 (2020) 107622.
[41] M. Mir, M. Tahani, Graphene-based mass sensors: Chaotic dynamics analysis using the nonlocal strain gradient model, Appl. Math. Model. 81 (2020) 799–817.
[42] L. Hadji, F. Bernard, N. Zouatnia, Bending and free vibration analysis of porous-functionally-graded (PFG) beams resting on elastic foundations, Fluid Dynamic and Material Process 19 (4) (2023) 1043–1054.
[43] M. Dahmane, L. Noureddine, A.S. Benosman, R. Bennai, H.A. Atmane, M. Benadouda, Inclined crack identification in bidirectional FG beams on an elastic foundation using the h-version of the finite element method, Mech. Adv. Mater. Struct. (2023), https://doi.org/10.1080/15376494.2023.2290226.
[44] M. Dahmane, M. Benadouda, A. Fellah, A. Saimi, A.A. Hassen, I. Bensaid, Porosities-dependent wave propagation in bi-directional functionally graded cantilever beam with higher-order shear model, Mech. Adv. Mater. Struct. (2023), https://doi.org/10.1080/15376494.2023.2253546.
[45] L. Hadji, A. Fallah, M.M. Aghdam, Influence of the distribution pattern of porosity on the free vibration of functionally graded plates, Struct. Eng. Mech. 82 (2) (2022) 151–161.
[46] R. Madan, S. Bhowmick, L. Hadji, A. Tounsi, Limit elastic speed analysis of rotating porous annulus functionally graded disks, Steel Compos. Struct. 42 (3) (2022) 375–388.
[47] A.S. Sayyad, P.V. Avhad, L. Hadji, On the static deformation and frequency analysis of functionally graded porous circular beams, Forces in Mechanics 7 (2022) 100093.
[48] L. Hadji, R. Madan, F. Bernard, Thermal buckling in multi-directional porous plates: the effects of material grading and aspect ratio, Proc. Inst. Mech. Eng. G J. Aerosp. Eng. 238 (4) (2024) 412–426.
[49] L. Hadji, V. Plevris, G. Papazafeiropoulos, Investigation of the static bending response of FGM sandwich plates, Journal of Applied and Computational Mechanics 10 (1) (2024) 26–37.
[50] Turan M, Uzun Yaylacı E, Yaylacı M. Free vibration and buckling of functionally graded porous beams using analytical, finite element, and artificial neural network methods. Arch. Appl. Mech. 203; 93: 1351-1372..
[51] H. Qing, L. Wei, Linear and nonlinear free vibration analysis of functionally graded porous nanobeam using stress-driven nonlocal integral model, Communications in Nonlinear Science and Numerical Simulation 109 (2022) 106300.
[52] M.A. Al-Zahrani, S.A. Asiri, K.I. Ahmed, M.A. Eltaher, Free vibration analysis of 2D functionally graded Strip beam using Finite element method, Journal of Applied and Computational Mechanics 8 (2022) 1422–1430.
[53] A. Gee, S.M. Hashemi, Undamped free vibration analysis of functionally graded beams: a dynamic finite element approach, Applied Mechanics 3 (2022) 1223–1239.
[54] Q.H. Pham, V.K. Tran, P.C. Nguyen, Hygro-thermal vibration of bidirectional functionally graded porous curved beams on variable elastic foundation using generalized finite element method, Case Stud. Therm. Eng. 40 (2022) 102478.
[55] A. Saimi, I. Bensaid, A. Fellah, Effect of crack presence on the dynamic and buckling responses of bidirectional functionally graded beams based on quasi-3D beam model and differential quadrature finite element method, Arch. Appl. Mech. 93 (2023) 3131–3151.
[56] P. Bridjesh, N.K. Geetha, B. Yelamasetti, Numerical investigation on buckling of two-directional porous functionally graded beam using higher order shear deformation theory, Int. J. Interact. Des. Manuf. (2023). https://doi.org/10.1007/s12008-023-01332-6.
[57] V.K. Nathi, Buckling analysis of 2D functionally graded porous beams using novel higher order theory, J. Comput. Appl. Mech. 53 (2022) 393–413.
[58] A. Karamanlı, Free vibration analysis of two directional functionally graded beams using a third order shear deformation theory, Compos. Struct. 189 (2018) 127–136.
[59] T.P. Vo, H.T. Thai, T.K. Nguyen, A. Maheri, J. Lee, Finite element model for vibration and buckling of functionally graded sandwich beams based on a refined shear deformation theory, Eng. Struct. 64 (2014) 12–22.
[60] Z. Xiao, Generalized Karush-Kuhn-Tucker conditions in variational and set-valued analysis, Optimization and Control (math.OC) 1 (2020) 1–39.
[61] Y. Ye, On the complexity of approximating a KKT point of quadratic programming, Math. Program. 80 (1998) 195–211.
[62] G. Reddy, N.V. Kumar, Free vibration analysis of 2D functionally graded porous beams using novel higher-order theory, Mechanics of Advanced Composite Structures 10 (2023) 69–84.
[63] T.P. Vo, H.T. Thai, T.K. Nguyen, F. Inam, Static and vibration analysis of functionally graded beams using refined shear deformation theory, Meccanica 49 (2014) 155–168.
[64] M.M. Keleshteri, J. Jelovica, Analytical assessment of nonlinear forced vibration of functionally graded porous higher order hinged beams, Compos. Struct. 298 (2022) 115994.
[65] A. Melaibari, S.A. Mohamed, A.E. Assie, R.A. Shanab, M.A. Eltaher, Free vibration characteristics of bidirectional graded porous plates with elastic foundations using 2D-DQM, Mathematics 11 (2022) 46.
[66] M. Galeban, A. Mojahedin, Y. Taghavi, M. Jabbari, Free vibration of functionally graded thin beams made of saturated porous materials, Steel Compos. Struct. 21 (2016) 999–1016.